Nonlinear Processes
in Geophysics
Discussions

Open Access

Local finite time Lyapunov exponent, local sampling and probabilistic source and destination regions

A. E. BozorgMagham[1], S. D. Ross[2], and D. G. Schmale III[3]

[1]Department of Atmospheric and Oceanic Science, University of Maryland, College Park, MD, 20742, USA
[2]Dept. of Biomedical Engineering and Mechanics, Virginia Tech, Blacksburg, VA 24061, USA
[3]Dept. of Plant Pathology, Physiology, and Weed Science, Virginia Tech, Blacksburg, VA 24061, USA

Correspondence to: A. E. BozorgMagham (amirb@atmos.umd.edu)

Discussion Paper | Discussion Paper | Discussion Paper | Discussion Paper |

NPGD

2, 903–937, 2015

Local finite time Lyapunov exponent

A. E. BozorgMagham et al.

Title Page

Abstract | Introduction

Conclusions | References

Tables | Figures

|◄ | ►|

◄ | ►

Back | Close

Full Screen / Esc

Printer-friendly Version

Interactive Discussion

Abstract

The time-varying finite time Lyapunov exponent (FTLE) is a powerful Lagrangian concept widely used for describing large-scale flow patterns and transport phenomena. However, field experiments usually have modest scales. Therefore, it is necessary to bridge between the powerful concept of FTLE and (local) field experiments. In this paper a new interpretation of the local FTLE, the time series of a FTLE field at a fixed location, is proposed. This concept can practically assist in field experiments where samples are collected at a fixed location and it is necessary to attribute long distance transport phenomena and location of source points to the characteristic variation of the sampled particles. Also, results of this study have the potential to aid in planning of optimal local sampling of passive particles for maximal diversity monitoring of assemblages of microorganisms. Assuming a deterministic flow field, one can use the proposed theorem to (i) estimate the differential distances between the source (or destination) points of the collected (or released) particles when consecutive sampling (or releasing) is performed at a fixed location, (ii) estimate the local FTLE as a function of known differential distances between the source (or destination) points. In addition to the deterministic flows, the more realistic case of unresolved turbulence and low resolution flow data that yield the probabilistic source (or destination) regions are studied. It is shown that similar to deterministic flows, Lagrangian coherent structures (LCS) separate probabilistic source (or destination) regions corresponding to consecutive collected (or released) particles.

1 Introduction

The classical interpretation of finite time Lyapunov exponent (FTLE) fields and the associated hyperbolic Lagrangian coherent structures (LCSs) provides useful information about large-scale flow patterns and transport and mixing phenomena in flow domains (Haller and Poje, 1998; Haller and Yuan, 2000; Mancho et al., 2004; Shadden et al.,

A. E. BozorgMagham et al.

Title Page

Abstract | Introduction

Conclusions | References

Tables | Figures

◄◄ | ►►

◄ | ►

Back | Close

Full Screen / Esc

Printer-friendly Version

Interactive Discussion

2005; Haller, 2011). There are an increasing number of studies that apply various concepts of LCSs, based on the classic right Cauchy–Green tensor, to describe and predict the time evolution of Lagrangian features in geophysical systems. In some of these studies, geophysical information (e.g., wind or oceanic velocity fields) have been used as the input data and Lagrangian results (e.g., the distribution of an oil spill in the ocean or volcanic ash in the atmosphere) over a large area are compared with the behavior of the geophysical system either via satellite data or simulations (Dellnitz et al., 2009; Peng and Peterson, 2012; Olascoaga and Haller, 2012; Mendoza and Mancho, 2012; Olascoaga et al., 2012). A large scale distribution of particles is a common characteristic among these studies. In contrast, this study is motivated by a series of field experiments and studies regarding the long distance transport of airborne microorganisms where only a limited number of localized (and temporally consecutive) measurements of the atmospheric structure of microbial assemblages is available (Schmale III et al., 2008; Tallapragada et al., 2011; Schmale et al., 2012; Lin et al., 2013). Therefore, there is a need to bridge the powerful concept of FTLE and (local) field experiments.

In this paper, we present a new interpretation of local FTLE using the concept of local Lyapunov exponents in ordinary differential equation systems (Abarbanel et al., 1992; Branicki and Wiggins, 2009) . The suggested interpretation of local FTLE helps us to investigate long distance transport phenomena as a possible cause of characteristic variation in successively collected airborne samples such as the presence or absence of a unique strain or species of microorganism. In addition, this analysis is useful for planning the atmospheric collections at a fixed location with respect to the forecast data of FTLE fields. Because this study is motivated by aerial measurements in realistic conditions, i.e., hundreds of collections of microorganisms from the atmosphere with drones, it is necessary to consider the spatiotemporal limitations of the available velocity field data. These limitations are manifested in unresolved turbulence and impose uncertainties on the location of the source and destination points. For this reason, we use a Lagrangian particle dispersion model to determine the probabilistic source (or destination) regions and show how the concept of local FTLE can explain the

Local finite time Lyapunov exponent

A. E. BozorgMagham et al.

degree of separation between probabilistic source (or destination) regions (Fay et al., 1995; Draxler and Hess, 1998; BozorgMagham and Ross, 2015), and may contribute to understanding the degree of geographic and genetic diversity observed in aerial samples.

⁵ Results of this study are important for practical environmental applications such as early warning and integrated risk management systems in agriculture communities and sampling planning from geophysical flows (Tallapragada et al., 2011; BozorgMagham et al., 2013; BozorgMagham and Ross, 2015).

This paper is outlined as follows. In Sect. 2 we define the local FTLE and study the
¹⁰ relationship between this concept and the dispersion of source (or destination) points in deterministic flow fields. In Sect. 3 we show some numerical verification and applications of the local FTLE concept. In Sect. 4 we consider the unresolved turbulence and investigate the uncertainty of the backward and forward trajectories and the resulting probabilistic source and destination regions.

¹⁵ **2 Local finite time Lyapunov exponent**

In this section we consider a new interpretation of local FTLE for a time-varying vector field, e.g., $dx/dt = v(x, t)$, which is conceptually related to the local Lyapunov exponent (LE) in ordinary differential equation (ODE) systems (Oseledec, 1968; Abarbanel et al., 1992). By local FTLE we mean the time-varying value of the FTLE field at an arbitrary
²⁰ location x. Classically, the time-varying FTLE measures the maximum separation rate between nearby particles when they are released in the flow field at the same time (isochrone particles). Figure 1 refers to this classical description. This figure shows two (isochrone) particles which are close to each other at an initial time t_0. Under the effect of the flow field the displacement vector between the two particles, δx, changes.
²⁵ After an elapsed time T, the new vector between the two particles is

$$\delta x(t_0 + T) = \phi_{t_0}^{t_0+T}(x + \delta x) - \phi_{t_0}^{t_0+T}(x) = D\phi_{t_0}^{t_0+T}(x) + O\left(\|\delta x(t_0)\|^2\right) \tag{1}$$

where $\phi_{t_0}^{t_0+T}$ is the flow map for the vector field from time t_0 to $t_0 + T$ and $D\phi_{t_0}^{t_0+T} = \mathrm{d}\phi_{t_0}^{t_0+T}(\boldsymbol{x})/\mathrm{d}\boldsymbol{x}$ is the Jacobian of the flow map.

The maximum possible separation between the released particles after time interval T, assuming sufficiently small initial distance between them with respect to an appropriate norm $\|\cdot\|$, is proportional to the square root of the maximum singular value, λ_{max}, of the right Cauchy–Green strain tensor, Δ.

$$\max\|\delta\boldsymbol{x}(t_0 + T)\| = \sqrt{\lambda_{max}(\Delta)}\|\delta\boldsymbol{x}(t_0)\| \tag{2a}$$

$$\Delta(\boldsymbol{x}, t_0, T) = D\phi_{t_0}^{t_0+T}(\boldsymbol{x})^{\mathsf{T}} D\phi_{t_0}^{t_0+T}(\boldsymbol{x}). \tag{2b}$$

The finite time Lyapunov exponent (FTLE), with t_0 and T fixed, is considered a scalar field of the Lyapunov exponent as a function of initial position, $\boldsymbol{x}$,

$$\sigma_{t_0}^{T}(\boldsymbol{x}) = \frac{1}{|T|}\ln\sqrt{\lambda_{max}(\Delta)}. \tag{3}$$

Similar to the calculation of maximum separation between two initially neighboring points in an ODE system and the corresponding maximum LEs, $\sigma_{t_0}^{T}$ is used to describe the $\max\|\delta\boldsymbol{x}(t_0 + T)\|$ as

$$\max\|\delta\boldsymbol{x}(t_0 + T)\| = \exp\left(\sigma_{t_0}^{T}(\boldsymbol{x}, t_0)|T|\right)\|\delta\boldsymbol{x}(t_0)\|. \tag{4}$$

In this study we are interested in particles that are sampled (or released) consecutively in time at a fixed location. Thus, the standard concept of the FTLE, i.e., separation rate of nearby isochron points, is not applicable. Therefore, we propose and apply the concept of local FTLE. We show that we can (i) recover an approximation of the true local FTLE by using the differential distances of the successive source (or destination) points and (ii) estimate the differential distance of the source (or destination) points by having the true local FTLE and (local) velocity time-series.

In the following sections we focus on the backward FTLE fields and the location of source points because this situation is important for our field studies for identifying potential source regions of plant pathogens and their relative risk of transport to previously unexposed regions Lin et al. (2014); Prussin et al. (2014b, a, 2015). However, all the results are valid for forward time FTLE fields as well, and the spread of passive particles released from a fixed location.

Theorem: providing sufficiently small time interval between successive sampling events, i.e., δt, and sufficiently long elapsed time, i.e., $|T| \gg \delta t$, the true local FTLE value, averaged over the time interval $[t_1, t_2]$, can be approximated by

$$\sigma^T_{[t_1,t_2]}(\boldsymbol{x}) = \lim_{\delta t \to 0} \frac{1}{|T|} \ln \frac{\delta(\boldsymbol{x}, T, t_1, \delta t)}{\|\overline{\boldsymbol{v}}(\boldsymbol{x}, t_1, t_2)\delta t\|}. \tag{5}$$

where t_1 and $t_2 = t_1 + \delta t$ are the times that particles 1 and 2 are observed at the sampling location $\boldsymbol{x}$, $|T|$ is the norm of the elapsed time, $\delta(\boldsymbol{x}, T, t_1, \delta t)$ is the distance between successive source points corresponding to the elapsed time T, and $\overline{\boldsymbol{v}}(\boldsymbol{x}, t_1, t_2)$ is the average velocity at the sampling location over $[t_1, t_2]$.

To prove this theorem, we introduce δ^* (shown by the dashed line in Fig. 2) which is the distance between particle 1 (shown by a solid circle) and particle 2 at time t_2. For clarity, we also view this backward time problem in the forward direction, from source point to sampling point. By satisfying two conditions, the above theorem is automatically converted to the classic interpretation of FTLE. Those two conditions are (i) δ^* is sufficiently small, (ii) $\delta(\boldsymbol{x}, T, t_1, \delta t)$ is close to the maximum separation between the two particles.

Proof: if the time between successive sampling (or release) events is sufficiently small ($\delta t \to 0$ or $\delta t \ll T_L$, the Lagrangian time scale of the velocity field) and the magnitude of the velocity at any arbitrary location is finite, then $\delta^* = \left\| \int_{t_1}^{t_2 = t_1 + \delta t} \boldsymbol{v}(\boldsymbol{x}, t)\, dt \right\|$ converges

Title Page

Abstract | Introduction

Conclusions | References

Tables | Figures

|◄ | ►|

◄ | ►

Back | Close

Full Screen / Esc

Printer-friendly Version

Interactive Discussion

to $\left\| \bar{v}(x, t_1, t_2)\delta t \right\|$, which is small. Therefore the first condition is satisfied. The total elapsed time for particle 1 from its source location to the solid circle is $T + \delta t$ which is approximately the same as the integration time of particle 2 since $T \gg \delta t$. Therefore, if we look in the reverse-time direction we can consider the two particles as nearly isochronic particles which are released from two nearby points (bold cross and solid circle), each with elapsed time T. To satisfy the second condition, we need to show that $\delta(x, T, t_1, \delta t)$ is close to the maximum possible distance between the two particles after T (referring to Eq. 4). In general, the direction of maximum expansion dominates the dynamics of the displacement vector growth (Rosenstein et al., 1993). Therefore any two nearby initial conditions will stretch into the direction of the local leading Lyapunov vector. Thus, with a sufficiently long elapsed time T we conclude that the two separated particles lie along (or very close to) the major axis of an ellipse which is generated by deformation of a sufficiently small sphere of arbitrary initial conditions (Tanaka and Ross, 2009). Thus, as $\delta t \to 0$ and for sufficiently large $|T|$, $\delta(x, T, t_1, \delta t)$ is sufficiently close to the maximum possible distance between the two particles. Therefore, the two necessary conditions are satisfied and the proof is completed. ∎

This theorem enables us to recover the local FTLE if we have the distance between the source points and the time-varying velocity at the sampling point. More importantly, for sampling purposes, the reverse is also true; we can use Eq. (5) to estimate the distance between the isochronic source positions of consecutively collected particles, provided we also have the velocity (e.g., wind velocity from an anemometer) and local FLTE data at the sampling location as

$$\delta(x, T, t_1, \delta t) = \exp\left(|T|\sigma^T_{(t_1, t_2)}(x)\right) \left\| \bar{v}(x, t_1, t_2)\delta t \right\|. \tag{6}$$

We note the following. (i) Results of this theorem are also valid for forward FTLE fields and spread of passive particles. In this case, sampling and source locations are replaced by release and destination locations respectively. (ii) Results of this theorem are independent of the flow field dimension. (iii) By decreasing the time interval be-

tween successive sampling (or releases) events, i.e., smaller δt, errors of Eqs. (5) and (6) decrease and the approximated local FTLE value and differential distance would be closer to the true values. (iv) A larger (true) local FTLE of the real flow field, yields smaller error of estimations for the recovered local FTLE and the differential distance.

5   In following section we demonstrate some numerical verification and applications of this theorem.

3   Numerical verification and some applications

3.1   Numerical verification of the local FTLE theorem

We apply the local FTLE theorem to compare the true (benchmark) and the recovered
10   local FTLE time-series and also the true and the estimated differential distances of the source locations corresponding to the particles that were sampled at Virginia Tech's Kentland Farm, located at $37°11'$ N and $80°35'$ W, where we have collected a large variety of microbial samples with drones over the past 7 years (2006 to 2013) (Schmale et al., 2012). We refer to this point as $(0,0)$ in our plots.
15   The flow maps are calculated by using numerical data corresponding to the North America Mesoscale, NAM–218 provided by the National Oceanic and Atmospheric Administration (NOAA) and National Centers for Environmental Prediction's (NCEP) Operational Model Archive and Distribution System (NOMADS) project[1]. Spatial resolution of this data set is about 12.1 km and the temporal resolution is 3 h. All the trajecto-
20   ries are calculated by a fourth order Runge–Kutta integrator with a constant integration time step equals to 5 min. We use third order splines for all necessary spatiotemporal interpolations. We consider the time interval 12:00 UTC 29 September to 12:00 UTC 30 September 2010 for our numerical experiments and refer to it as the *interrogation window*.

---

[1]http://nomads.ncdc.noaa.gov/data.php

Figure 3a and b shows the trajectories and the initial positions of the indexed particles corresponding to the collected particles at the sampling location during the interrogation window. The frequency of sampling was 1 h and the backward time integration is 24 h for all the particles. In addition, for simplicity and without losing generality of the results we perform the integration on a quasi-2-D 850 mb pressure surface (BozorgMagham and Ross, 2015). Indices of this figure indicate the sampling times of the collected particles, for example index "12" that locates on the North-West of the figure refers to the initial position of a particle that started at 12:00 UTC 28 September and was collected 24 h later, i.e., 12:00 UTC 29 September, at the sampling location. In terms of streaklines (Batchelor, 2000), this line (Fig. 3b) is composed of contemporaneous points, e.g., 24 h, from the assembly of streaklines which pass through the sampling location during the interrogation window. We define this line as the *isochron source-line* since the integration time from all points on it to the sampling location is the same, i.e., 24 h in this example.

Following the assumptions of the local FTLE theorem ($\delta t \ll T_L$, the Lagrangian time scale of the velocity field, which is in the order of approximately 10^4 s for the horizontal turbulence cases, Draxler and Hess, 1998), we have to choose small sampling periods. For this aim the frequency of sampling, δt, is selected from 0.1 to 1 h and all the integrations are done in the same interrogation window. Figure 4a shows the benchmark (true) differential distance between successive source points, i.e., $\delta(\boldsymbol{x}, T, t_1, t_2)$, during the interrogation window calculated from the available velocity field data. We use the average velocity at the sampling location to calculate δ^* as $\left\| \overline{\boldsymbol{v}}(\boldsymbol{x}, t_1, t_2) \delta t \right\|$. In general, the average velocity term, i.e., $\overline{\boldsymbol{v}}(\boldsymbol{x}, t_1, t_2)$, is approximated by the average of the velocities at two successive sampling (or release) times or the velocity at the mid time of two sampling (or release) events. Figure 4b show the time series of the recovered local FTLE time-series for each sampling case, assuming that the true successive differential distances are available.

Figures 3b and 4 demonstrate that we interpret a *local (backward) FTLE time-series as differential stretching of line elements, i.e., strain, along an isochron source-line*. To

Local finite time Lyapunov exponent

A. E. BozorgMagham et al.

Title Page

Abstract | Introduction

Conclusions | References

Tables | Figures

◀ | ▶|

◀ | ▶

Back | Close

Full Screen / Esc

Printer-friendly Version

Interactive Discussion

verify this result and to study the effect of different δt's on the recovery of local FTLE time-series we calculate the benchmark backward FTLE fields for the interrogation window with integration time equal to 24 h. Figure 5a shows an image of the time-varying FTLE field corresponding to 12:00 UTC 29 September 2010. To give a sense about the changes of the FTLE field during the interrogation window, we may describe the motion of the strong ridges of the field in Fig. 5a toward North-West direction (upper-left corner of the figure as shown by the arrow). Figure 5b shows the benchmark (true) local FTLE value (black line) at the Kentland Farm during the interrogation window. To generate this plot we calculate the backward FTLE field every 15 min, then the time varying value of FTLE at $(0,0)$ is extracted. Also for comparing the results, the recovered FTLE time-series corresponding to $\delta t = 0.1$ h is displayed in the same panel by the red line. Figures 4b and 5b indicate that: (i) by choosing smaller sampling period time, δt, the recovered local FTLE time-series converges to the true one. (ii) The estimation error is smaller for larger values of the true local FTLE. Therefore, when $\sigma \rightarrow 0$ we may observe larger errors of estimation, e.g., between 00:00 and 04:00 UTC in Fig. 5b. For $\delta t = 0.1$ h we observe that the two time series are highly correlated and also their maxima (corresponding to the local maxima of the FTLE field) are at the same times (within $\delta t = \pm 0.1$ h). Therefore, for sufficiently small δt's the recovered local FTLE time-series can accurately capture the passage times of moving ridges of a FTLE field. Detecting those ridges is important since they are candidates for hyperbolic LCSs in many geophysical applications (Tallapragada et al., 2011; Haller, 2011; Karrasch, 2012; BozorgMagham et al., 2013).

In addition, we investigate whether we can estimate the differential distances by the local FTLE theorem providing necessary information about local velocity and FTLE. Figure 6 is a numerical example that shows that the benchmark differential distance between the successive source points (black line) is well approximated by the local FTLE theorem as $[4]\delta = \exp(|T|\sigma_{[t_1,t_2]}^{T}(\boldsymbol{x}))\|\overline{\boldsymbol{v}}(\boldsymbol{x},t_1,t_2)\,\delta t\|$ which is shown by the red line. Note that in this case we have the data of the true local FTLE and the local velocity. In this figure we see that with $\delta t = 0.25$ h, the estimated differential distance

time-series is very similar to the true answer and it captures the correct times of the local maxima. This is an empirically important result, because one can schedule the sampling from geophysical flows based on the available forecast FTLE fields and local velocity such that the successive collected particles originate from the most possible diverse locations (see Sect. 3.2). In Fig. 6 it is evident that there are two optimal time intervals, i.e., before and after 16:00 UTC, for maximal diversity monitoring. To interpret this, consider Fig. 3b and notice that the geographic extent of the line segment from point 15 to point 16 is much larger than segment 13 and 14.

3.2 Applications of the local FTLE theorem

A direct result of the local FTLE recovery theorem is the possibility of planning for maximal geographic (and therefore also genetic) diversity monitoring such that the collected particles come from the most separated source locations. This means incorporating greater potential source areas, which could drive a greater diversity of sample collection.

Suppose that it is desired to maximize the genetic diversity of microorganisms collected in a sample, assuming that all the sampled particles have approximately the same flight time. Results of the local FTLE theorem indicate that the optimal time for collecting samples such that they originate from the most possible distant locations is at times corresponding to the maxima of the local FTLE time-series (note the high correlation between the differential distance and the local FTLE time-series in Figs. 6 and 5b). To ensure that the particles are coming from significantly separated locations we may use the topology of the FTLE field and collect the samples on either side of a strong attracting LCS feature which corresponds to a local maximum of $\sigma_{[t_1,t_2]}^T$, providing short enough time between sampling periods. In this condition, high value of $\sigma_{[t_1,t_2]}^T$ as the exponent in Eq. (4) is the reason for having a large δ. Figure 7 schematically shows this strategy when an attracting LCS feature passes over a fixed sampling location causing a dramatic change in the region of possible source points of collected particles.

913

As an example in realistic geophysical flow, Fig. 8 shows trajectories of three hypothetical particles that are collected at $(0, -100)$ km with respect to the reference point. Backward integration time for specifying the corresponding source points, i.e., A, B and C, and the trajectories is 40 h for those three particles. The sampling times during the interrogation window are 13:40 UTC for the red particle, 14:00 UTC for the blue particle and 14:10 UTC for the green particle. The green and the blue particles are sampled on one side of an attracting LCS but the red particle is sampled on the other side of the same LCS. As we observe, the source points corresponding to blue and green particles, points B and C, are close meanwhile the source point of the red particle, point A, is significantly far from the other two particles. An interesting feature of this figure is that the separation of the trajectories does not start from the sampling point, but as it is shown, the three trajectories remain close to each other for about 200 km and then begin to diverge. This observation is directly related to the concept of the FTLE, because $\sigma_{t_0}^T$ is a function of the "final" separation between nearby particles and it does not specify the moment of divergence.

Referring to this example, the local FTLE theory can help us to explain the observation of significant characteristic variation of the collected particles, e.g., genetic types or aerial density of the microbial samples, at the sampling location during short intervals when sampling is coincide with a high value local FTLE, or equivalently, passage of a strong LCS over the sampling location (Tallapragada et al., 2011; Lin et al., 2013). In addition, a direct result of the local FTLE theorem is that when the local FTLE value is small during the sampling process, then it is expected that the collected particles originate from nearby source points, assuming approximately same flight times for them. This might be the reason that the characteristics of the microbial samples remain quasi-constant in consecutive collections, but differ as the time between sample collections increases (Lin et al., 2013). This situation is similar to sampling from a coherent set where the FTLE values are generally small (Froyland et al., 2010; Tallapragada and Ross, 2013) and the particles have similar Lagrangian characteristics. Moreover, in cases that we observe significant changes in collected samples while local FTLE value

is small, we may conclude that those changes are caused by some local incidents rather than long range transport phenomena (Lin et al., 2013). Thus, the local FTLE concept helps us to include or exclude rare/unique microbes from specific source regions.

4 Unresolved turbulence and probabilistic regions

In this section we study the uncertainty in calculation of the source (or destination) points due to the unresolved turbulence and also the role of high-value local FTLE in separation of the probabilistic source (or destination) regions.

Precise calculation of the source (or destination) point of any collected (or released) particle and the corresponding flow map require high resolution data of the velocity field. But geophysical data are always discrete and spatially sparse. For example, spatial and temporal resolution of operational data set varies from the order of 10 to hundreds of kilometers and 3 h to longer intervals respectively. Meanwhile, spatiotemporal scales of atmospheric flows can be smaller than the resolution of the available data and we may lose important Lagrangian phenomena such as turbulent diffusion and small size eddies if we just consider available data (Csanady, 1973; Rodean, 1996). Therefore, for realistic calculation of the source (or destination) points it is necessary to consider the the uncertainty of the trajectories. For this purpose, we consider a Lagrangian particle dispersion model (LPDM) that provides the stochastic component of the velocity with respect to the available deterministic (background) data (Legg and Raupach, 1982; Fay et al., 1995; Draxler and Hess, 1998; Stohl et al., 2005). The overall velocity $v(x,t)$ is composed of a deterministic term, $\overline{v}(x,t)$, and a random variable, $V(x,\overline{v},t)$, which depends explicitly on the instantaneous position of the particle x, its deterministic velocity $\overline{v}$ at that location and the time t; see Eq. (7). Later, we see how this dependency dictates two different solutions for the calcualtions of the probabilistic source and destination regions (BozorgMagham and Ross, 2015).

$$v(x,t) = \overline{v}(x,t) + V(x,\overline{v},t). \tag{7}$$

The stochastic term of the Eq. (7) is a Markov-chain process as a function of the velocity deformation tensor and the Lagrangian time scale of the flow field,

$$V_{(t+\Delta t)} = R_{\Delta t} V_t + \left(1 - R_{\Delta t}^2\right)^{0.5} \mathcal{N}(0,1) \sqrt{\kappa/T_L} \qquad (8)$$

where V shows each component of the stochastic velocity term $\boldsymbol{V}$, and the correlation coefficient $R_{\Delta t}$ is a measure of the association between stochastic velocities during successive time steps. Also, $\mathcal{N}$ is a normal distribution with mean zero and unit SD. The correlation coefficient

$$R_{\Delta t} = \exp\left(-\Delta t/T_{\mathrm{L}}\right). \qquad (9)$$

is a function of integration time step, Δt, and the Lagrangian time scale of the flow field, T_{L}, which is on the order of 10^4 s. The term κ depends on the gradient of the instantaneous deterministic velocity, $\overline{\boldsymbol{v}} = (\overline{u}, \overline{v})$, the meteorological data grid size, χ, and an empirical constant, c,

$$\kappa = 2^{-0.5}(c\chi)^2 \left[\left(\frac{\partial \overline{v}}{\partial x} + \frac{\partial \overline{u}}{\partial y}\right)^2 + \left(\frac{\partial \overline{u}}{\partial x} - \frac{\partial \overline{v}}{\partial y}\right)^2\right]^{0.5}. \qquad (10)$$

Because κ depends on the gradient of the background velocity one can use the set of Eqs. (7)–(10) for forward integration. Using this set for simple backward integration requires presumption about the position of a particle at specific times which leads to misleading results. Therefore, we have to consider two distinct cases, (i) calculation of the probabilistic destination region of a released particle, (ii) calculation of the probabilistic source region of a collected particle. In this study we discuss both cases, but like before, emphasize the probabilistic source regions (corresponding to the backward trajectories). We also revisit the problem of local FTLE and successive sampling when the effects of unresolved turbulence are considered. Our numerical results show that even in the presence of unresolved turbulence, if successive sampling are performed

Local finite time Lyapunov exponent

A. E. BozorgMagham et al.

on either side of a strong attracting LCS, then the probabilistic source regions are significantly separated similar to the deterministic case.

To focus on the main concerns of this study and to avoid complexity we proceed with a 2-D velocity field similar to the previous sections. However, this approach can be extended to 3-D fields by adding an appropriate stochastic term in the extended direction (Rodean, 1996).

4.1 Probabilistic source and destination regions

(i) The probabilistic destination region is the probability distribution of the final positions of virtually released particles after integration time T when the initial position is known precisely, e.g., a Dirac delta function. The case of forward integration and related calculations of a probabilistic distribution is equivalent to solving the Fokker–Planck or Kolmogorov forward equations (Rodean, 1996; Risken, 1985) which describe the future of a probability distribution function of a known initial condition that evolves under the dynamics of a system, e.g., a diffusion process.

Because the time-varying vector fields are usually complicated, analytical solutions for probabilistic destination regions are not available and it is necessary to use numerical solutions. For this aim, we discretize the domain of our interest into sufficiently small boxes and then use the Monte Carlo method by releasing sufficient number of independent particles from a box that includes the release point. Figure 9 shows this procedure. By choosing an appropriate integration time step we calculate the trajectories. By completion of the integration process we have a distribution of particles in different boxes. If the total number of released particles is sufficiently large and the boxes' dimensions are sufficiently small, then the ratio of the virtual particles in each box to the total number of released particles show the probability distribution of the destination region. By increasing the number of virtual particles and decreasing the size of the boxes the calculated distribution becomes invariant.

(ii) The solution for a probabilistic source region is conceptually the same as solving the Kolmogorov backward problem (Risken, 1985). In mathematical terms, at time

Title Page

Abstract | Introduction

Conclusions | References

Tables | Figures

|◀ | ▶|

◀ | ▶

Back | Close

Full Screen / Esc

Printer-friendly Version

Interactive Discussion

$t_0 - T$ ($T > 0$ is the integration time) we investigate for a specific source distribution such that in a future time, i.e., t_0, the system will be in a given target set, i.e., the box that includes the sampling location. A probabilistic source region cannot be determined by simply performing backward time-integration. Because κ in Eq. (10) and consequently the stochastic velocity term are determined by the instantaneous background velocity which depends on the location and time. Naively applying the backward time-integration produces a series of "false" displacement vectors. The cumulative effect of these false displacements yields a false probabilistic source region. To solve this problem, we first discretize the domain of the flow field into small boxes. Then, we shift the starting time to $t_0 - T$. By this means, we convert this problem into a forward integration problem from $t_0 - T$ to t_0. At $t_0 - T$ we release a sufficient number of independent (virtual) particles from all boxes of the domain (this step is the major difference between the current and the previous case). By forward integration from $t_0 - T$ to time t_0 we find the landing location of all released particles. The influential particles in this procedure are those which land inside the sampling box, e.g., the green trajectories in Fig. 10. In this figure, those boxes that have contribute to the particles ending up in the target box, labeled "j", are hatched. As we observe, there may be particles from contributing boxes that do not land in the target box (shown by red trajectories).

In Fig. 10 the boxes are labeled by $i = 1, 2, \ldots, n_b$ where n_b is the number of boxes and the sampling box is shown by index j. We denote the number of particles which start from box i at time $t_0 - T$ and are in box j at time t_0 by $n_{i \to j}$. We calculate the relative contribution of each source box as,

$$\gamma_i = \frac{n_{i \to j}}{\sum_i n_{i \to j}}, \tag{11}$$

where $\sum_i n_{i \to j}$ shows the total number of particles that land in the sampling (target) box j and γ_i is the chance of a sampled particle to come from a specific box i. Therefore, the distribution of γ over the domain approximates the probability distribution of the source region. This procedure generates the correct probabilistic source region but its

numerical efficiency is not high because many, e.g., 10^6, independent particles are released from all boxes of the domain but only those particles that land in the sampling box are counted. Thus, there are a huge number of calculated trajectories that are left out. It is not the purpose of this study, but one can increase the efficiency of this procedure by applying some optimization methods. For example, sequential release of particles from large boxes that are inside a circle centered at the sampling box and identifying the regions with maximum contributions. The radius of that circle can be determined by statistical information about the mean velocity and the integration time. After that, one may focus on those important regions by partitioning them into smaller boxes and increasing the number of released particles to determine finer structures of the probabilistic source region. For more information regarding this problem one can refer to STILT project[2] (Lin et al., 2003; Nehrkorn et al., 2010; Hegarty et al., 2013).

4.2 Probabilistic source region and local FTLE

For a realistic example of probabilistic source regions and the local FTLE we revisit the case study of section Sect. 3.2. Figure 11a shows one example of a probabilistic source region where the color intensity shows the relative contribution of each source box. In this case the sampling location is at $(0, -100)$ km with respect to our reference point. Sampling time is 14:10 UTC 29 September 2010 and the total elapsed time for trajectory calculations is $T = 40$ h. This figure is the stochastic equivalent of the source point of the particle that its trajectory is shown by a green line in Fig. 8. For this calculation 10^5 particles are released from each 10 km × 10 km box. The search area for this specific problem is a 900 km × 600 km rectangular grid. Considering the size of the boxes, we would have 5400 of them. Therefore, the total number of released particles and calculated trajectories is 5.4×10^8 in each integration time step.

An important point for both cases, the probabilistic source and destination regions, is that although at each time step the stochastic velocity term has a Gaussian distri-

---

[2]http://www.stilt-model.org

A. E. BozorgMagham et al.

bution (recalling Eq. 8), the final distribution of particles is not necessarily Gaussian. The reason for this fact is the cumulative effects of the variability of the variance of normal distribution, $\sqrt{\kappa/T_{\mathrm{L}}}$, that is a function of the gradient of instantaneous velocity. In general, for small integration time the probability distribution of the source (or desti-

5 nation) region is close to a Gaussian distribution but as the integration time increases, the corresponding distribution diverges from a normal one. For example, visual inspection of Fig. 11b indicates that the final distribution of the probable source points is not Gaussian. In Fig. 11c the relative contribution of the source boxes along the specified line PQ is shown. Standard statistical tests such as the Kolmogorov–Smirnov test

10 (Lilliefors, 1967) confirm that the distribution is not Gaussian.

In Fig. 8 we show that the source locations of two sampled particles on either side of a attracting LCS are much further apart than the source points of two successive sampled particles on one side of the same LCS. We want to investigate whether this result is still valid in the presence of unresolved turbulence. If that result holds then

15 in practical applications such as sampling the microbial structure of the atmosphere we can have reasonable confidence about the separation of the probabilistic source regions based solely on a deterministic analysis, that is, without performing bothersome probabilistic calculations. We study this problem for an example for which we also know the deterministic answer. Figure 12 shows the evolution of the probabilistic source

20 regions "A" and "B" (shown in panel a) corresponding to red and blue particles of Fig. 8 respectively. The total integration time for this example is 40 h. In each panel of this figure we also show the contemporaneous attracting hyperbolic LCSs according to Haller (2011) and Karrasch (2012). For calculation of each probabilistic region of this figure, 10^5 particles are released from each small 10 km × 10 km box. By comparing

25 Fig. 8 and panel a of Fig. 12 we observe that the probabilistic source regions contain the deterministic source points and they significantly separated from each other. Also, we see how the two probabilistic regions contract and become closer to the attracting LCS as they get closer to the sampling point. One noticeable feature in this figure is

the difference between the shapes of the two source regions, while the two sampling are separated by only 20 min.

Results of this example show that, similar to the deterministic case, the probabilistic source regions corresponding to the collected particles on either side of a deterministic attracting LCSs are significantly separated in backward time.

5 Conclusions

FTLE fields provide useful information about large-scale transport phenomena and also Lagrangian structures of flow fields. However, in field experiments the data are on a much more modest scale. Therefore, it is necessary to bridge the gap between the concept of FTLE and local experiments. Our new interpretation of local FTLE was motivated in part by our previous work examining the dynamics of assemblages of microorganisms in the lower atmosphere The mathematical concept of local FTLE enables us to either (i) estimate the differential distances between the source (or destination) points of successive collected (or released) particles assuming the availability of the local velocity and FTLE data, or (ii) recover an approximation of the the true local FTLE time-series if we have the local velocity and differential distance data.

The suggested notion is useful in practical cases where we have a collection of particles, sampled at a fixed location, and we want to generate hypotheses about the characteristics of the collected particles, their source locations and long distance transport phenomena. We show that assuming short time interval between successive sample collections, the differential distance between the corresponding source locations is described by the local FTLE (at sampling interval) and the local velocity. This result may help us to explain the variations in the genetic structure of assemblages of microorganisms in the atmosphere.

In addition, we show that the concept of local FTLE could be applied to scheduling of atmospheric sampling missions with drones to collect samples with a high diversity and/or that contain unique individuals or species. We also investigate the unresolved

Full Screen / Esc

Printer-friendly Version

Interactive Discussion

turbulence and the probabilistic description of the source (or destination) points. We use the box discretization method and discuss the important differences between calculation methods of the probabilistic source and destination regions. Furthermore, we show that because the stochastic velocity is a function of instantaneous background velocity, the probabilistic source (or destination) regions are not necessarily Gaussian. Finally, we study the probabilistic source regions corresponding to successive sampled particles on either side of a strong hyperbolic attracting LCS and we show that the source regions are significantly separated similar to the deterministic flow field.

Results of this study can aid in optimizing the sampling schedules of passive particles and also aid in understanding of the outcomes of local observations in geophysical flows, based on larger scale features.

References

Abarbanel, H. D., Brown, R., and Kennel, M. B.: Local Lyapunov exponents computed from observed data, J. Nonlinear Sci., 2, 343–365, 1992. 905, 906

Batchelor, G. K.: An Introduction to Fluid Dynamics, Cambridge University Press, 2000. 911

BozorgMagham, A. E. and Ross, S. D.: Atmospheric Lagrangian coherent structures considering unresolved turbulence and forecast uncertainty, Commun. Nonlinear Sci., 22, 964–979, 2015. 906, 911, 915

BozorgMagham, A. E., Ross, S. D., and Schmale, D. G.: Real-time prediction of atmospheric lagrangian coherent structures based on uncertain forecast data: an application and error analysis, Physica D, 258, 47–60, 2013. 906, 912

Branicki, M. and Wiggins, S.: Finite-time Lagrangian transport analysis: stable and unstable manifolds of hyperbolic trajectories and finite-time Lyapunov exponents, arXiv:0908.1129, 2009. 905

Csanady, G. T.: Turbulent Diffusion in the Environmnet, Vol. 3, Springer Science & Business Media, 1973. 915

Dellnitz, M., Froyland, G., Horenkamp, C., Padberg-Gehle, K., and Sen Gupta, A.: Seasonal variability of the subpolar gyres in the Southern Ocean: a numerical investigation based on transfer operators, Nonlin. Processes Geophys., 16, 655–663, doi:10.5194/npg-16-655-2009, 2009. 905

Draxler, R. and Hess, G.: An overview of the HYSPLIT_4 modelling system for trajectories, dispersion and deposition, Aust. Meteorol. Mag., 47, 295–308, 1998. 906, 911, 915

Fay, B., Glaab, H., Jacobsen, I., and Schrodin, R.: Evaluation of Eulerian and Lagrangian atmospheric transport models at the Deutscher-Wetterdienst using ANATEX surface tracer data, Atmos. Environ., 29, 2485–2497, 1995. 906, 915

Froyland, G., Lloyd, S., and Santitissadeekorn, N.: Coherent sets for nonautonomous dynamical systems, Physica D, 239, 1527–1541, 2010. 914

Haller, G.: A variational theory of hyperbolic Lagrangian Coherent Structures, Physica D, 240, 574–598, 2011. 905, 912, 920

Haller, G. and Poje, A.: Finite time transport in aperiodic flows, Physica D, 119, 352–380, 1998. 904

Haller, G. and Yuan, G.: Lagrangian coherent structures and mixing in two-dimensional turbulence, Physica D, 147, 352–370, 2000. 904

Hegarty, J., Draxler, R. R., Stein, A. F., Brioude, J., Mountain, M., Eluszkiewicz, J., Nehrkorn, T., Ngan, F., and Andrews, A.: Evaluation of Lagrangian particle dispersion models with measurements from controlled tracer releases, J. Appl. Meteorol. Clim., 52, 2623–2637, 2013. 919

Karrasch, D.: Comment on "A variational theory of hyperbolic Lagrangian coherent structures, Physica D 240 (2011) 574–598", Physica D, 241, 1470–1473, 2012. 912, 920

Legg, B. and Raupach, M.: Markov-chain simulation of particle dispersion in inhomogeneous flows – the mean-drift velocity induced by a gradient in Eulerian velocity variance, Bound.-Lay. Meteorol., 24, 3–13, 1982. 915

Lilliefors, H. W.: On the Kolmogorov–Smirnov test for normality with mean and variance unknown, J. Am. Stat. Assoc., 62, 399–402, 1967. 920

Lin, B., BozorgMagham, A. E., Ross, S. D., and Schmale, D. G.: Small fluctuations in the recovery of fusaria across consecutive sampling intervals with unmanned aircraft 100 m above ground level, Aerobiologia, 29, 45–54, 2013. 905, 914, 915

Lin, B., Ross, S. D., Prussin, A. J., and Schmale, D. G.: Seasonal associations and atmospheric transport distances of fungi in the genus *Fusarium* collected with unmanned aerial vehicles and ground-based sampling devices, Atmos. Environ., 94, 385–391, 2014. 908

Lin, J., Gerbig, C., Wofsy, S., Andrews, A., Daube, B., Davis, K., and Grainger, C.: A near-field tool for simulating the upstream influence of atmospheric observations: the Stochastic Time-Inverted Lagrangian Transport (STILT) model, J. Geophys. Res.-Atmos., 108, 4493, doi:10.1029/2002JD003161, 2003. 919

Mancho, A. M., Small, D., and Wiggins, S.: Computation of hyperbolic trajectories and their stable and unstable manifolds for oceanographic flows represented as data sets, Nonlin. Processes Geophys., 11, 17–33, doi:10.5194/npg-11-17-2004, 2004. 904

Mendoza, C. and Mancho, A. M.: Review Article: "The Lagrangian description of aperiodic flows: a case study of the Kuroshio Current", Nonlin. Processes Geophys., 19, 449–472, doi:10.5194/npg-19-449-2012, 2012. 905

Nehrkorn, T., Eluszkiewicz, J., Wofsy, S. C., Lin, J. C., Gerbig, C., Longo, M., and Freitas, S.: Coupled weather research and forecasting–stochastic time-inverted lagrangian transport (WRF–STILT) model, Meteorol. Atmos. Phys., 107, 51–64, 2010. 919

Olascoaga, M. J. and Haller, G.: Forecasting sudden changes in environmental pollution patterns, P. Natl. Acad. Sci. USA, 109, 4738–4743, 2012. 905

Olascoaga, M. J., Brown, M. G., Beron-Vera, F. J., and Koçak, H.: Brief communication "Stratospheric winds, transport barriers and the 2011 Arctic ozone hole", Nonlin. Processes Geophys., 19, 687–692, doi:10.5194/npg-19-687-2012, 2012. 905

Oseledec, V. I.: A multiplicative ergodic theorem. Lyapunov characteristic numbers for dynamical systems, Trans. Moscow Math. Soc., 19, 197–231, 1968. 906

Peng, J. and Peterson, R.: Attracting structures in volcanic ash transport, Atmos. Environ., 48, 230–239, 2012. 905

Prussin, A. J., Li, Q., Malla, R., Ross, S. D., and Schmale, D. G.: Monitoring the long distance transport of *Fusarium graminearum* from field-scale sources of inoculum, Plant Disease, 98, 504–511, 2014a. 908

Local finite time Lyapunov exponent

A. E. BozorgMagham et al.

Title Page

Abstract | Introduction

Conclusions | References

Tables | Figures

|◄ | ►|

◄ | ►

Back | Close

Full Screen / Esc

Printer-friendly Version

Interactive Discussion

Prussin, A. J., Szanyi, N. A., Welling, P. I., Ross, S. D., and Schmale, D. G.: Estimating the production and release of ascospores from a field-scale source of *Fusarium graminearum* inoculum, Plant Disease, 98, 497–503, 2014b. 908

Prussin, A. J., Marr, L. C., Schmale, D. G., Stoll, R., and Ross, S. D.: Experimental validation of a long-distance transport model for plant pathogens: application to *Fusarium graminearum*, Agr. Forest Meteorol., 203, 118–130, 2015. 908

Risken, H.: The Fokker-Planck equation: methods of solution and applications, Springer-Vlg, 1985. 917

Rodean, H. C.: Stochastic Lagrangian models of turbulent diffusion, Meteorological Monographs, 26, 1–84, doi:10.1175/0065-9401-26.48.1, 1996. 915, 917

Rosenstein, M. T., Collins, J. J., and De Luca, C. J.: A practical method for calculating largest Lyapunov exponents from small data sets, Physica D, 65, 117–134, 1993. 909

Schmale III, D. G., Dingus, B. R., and Reinholtz, C.: Development and application of an autonomous unmanned aerial vehicle for precise aerobiological sampling above agricultural fields, J. Field Robot., 25, 133–147, 2008. 905

Schmale, D. G., Ross, S. D., Fetters, T., Tallapragada, P., Wood-Jones, A., and Dingus, B.: Isolates of *Fusarium graminearum* collected 40 to 320 meters above ground level cause Fusarium head blight in wheat and produce trichothecene mycotoxins, Aerobiologia, 28, 1–11, 2012. 905, 910

Shadden, S. C., Lekien, F., and Marsden, J. E.: Definition and properties of Lagrangian coherent structures from finite-time Lyapunov exponents in two-dimensional aperiodic flows, Physica D, 212, 271–304, 2005. 904

Stohl, A., Forster, C., Frank, A., Seibert, P., and Wotawa, G.: Technical note: The Lagrangian particle dispersion model FLEXPART version 6.2, Atmos. Chem. Phys., 5, 2461–2474, doi:10.5194/acp-5-2461-2005, 2005. 915

Tallapragada, P. and Ross, S. D.: A set oriented definition of finite-time Lyapunov exponents and coherent sets, Commun. Nonlinear Sci., 18, 1106–1126, 2013. 914

Tallapragada, P., Ross, S. D., and Schmale, D. G.: Lagrangian coherent structures are associated with fluctuations in airborne microbial populations, Chaos, 21, 033122, doi:10.1063/1.3624930, 2011. 905, 906, 912, 914

Tanaka, M. L. and Ross, S. D.: Separatrices and basins of stability from time series data: an application to biodynamics, Nonlinear Dynam., 58, 1–21, 2009. 909
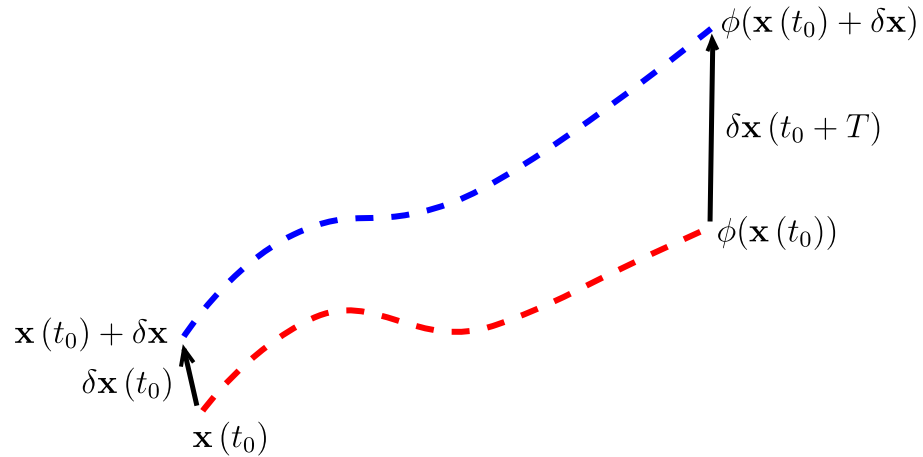
Figure 1. Separation of nearby particles during time interval T due to the flow map ϕ. The two particles are released in the flow field at the same time t_0; isochrone particles.

Figure 2. Two successive sampled particles at a fixed location shown by a bold cross. Particles 1 and 2 are collected at t_1 and $t_2 = t_1 + \delta t$ respectively (time interval between the two successive sampling is δt). The integration time between the sources and the sampling location is T for both particles. The excessive displacement of the first particle during δt is shown by δ^*.

Full Screen / Esc

Printer-friendly Version

Interactive Discussion

Figure 3. (a) Trajectories of the sampled particles during 24 h of integration. **(b)** Sequential source points and the isochron source-line. Sampling frequency is one hour between 12:00 UTC 29 September to 12:00 UTC 30 September 2010 and the sampling location is at (0,0) (Virginia Tech Kentland Farm 37°11′ N and 80°35′ W).

Full Screen / Esc

Printer-friendly Version

Interactive Discussion

Figure 4. (a) δ as the benchmark (true) differential distance between successive source points. Horizontal axis represents the averaged time corresponding to each successive pairs, **(b)** recovered local FTLE for different δt's form 0.1 h (6 min) to 1 h. Interrogation window is 12:00 UTC 29 September to 12:00 UTC 30 September 2010.

Figure 5. (a) The frozen image corresponding to 12:00 UCT 29 September 2010 of the backward FTLE field during the interrogation window. Integration time is 24 h for FLTE calculations. The bold arrow shows the general wind direction and the motion of the attracting LCS. **(b)** The true (black) and recovered (red) local FTLE time-series at the reference point (0,0). For the recovered time series (red), δt is equal to 0.1 h.
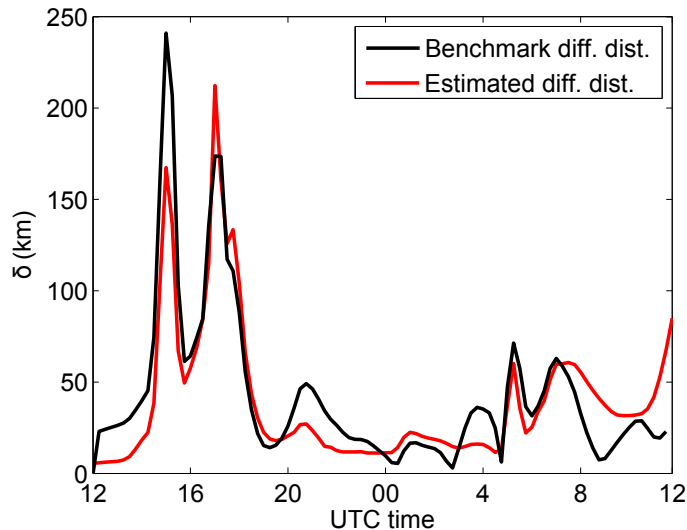
Figure 6. Differential distance between the successive source points on the isochron source-line corresponding to $\delta t = 0.25\,\text{h}$. The black line shows the benchmark and the red line shows the approximated time series which is calculated by local FTLE theorem as $\exp(|T|\sigma_{[t_1,t_2]}^{T}(\boldsymbol{x}))\|\overline{\boldsymbol{v}}(\boldsymbol{x},t_1,t_2)\delta t\|$. The backward integration time for calculations of the flow maps is $T = 24\,\text{h}$ and the interrogation window is 12:00 UTC 29 September to 12:00 UTC 30 September 2010.

Discussion Paper | Discussion Paper | Discussion Paper | Discussion Paper

Figure 7. An attracting LCS feature (red) passes over the sampling location (indicated by a bold ×). Dashed lines show trajectories of hypothetical particles that are absorbed to a moving attracting LCS. The bold arrow shows the general wind direction and the motion of the attracting LCS at the specified interval. Collected samples on either side of this attracting LCS feature come from two different regions.

Figure 8. Three trajectories of hypothetical collected samples. The red and blue trajectories correspond to the samples on either side of a LCS. The blue and green trajectories correspond to the samples on one side of the same LCS. Sampling times are 13:40, 14:00 and 14:10 UTC during the interrogation window (12:00 UTC 29 September to 12:00 UTC 30 September 2010) for the red, blue and the green particles, respectively. Source points of the sampled particles are shown by (A), (B), and (C). Integration time for all three particles is $T = 40$ h.

Figure 9. A solution for probability distribution of a forward case. Virtual particles are released from a box that includes the release location. Distribution of the final positions after integration time T would specify the probabilistic destination region. Calculation of the probabilistic destination region is equivalent to the solution of a Fokker–Planck equation for finding the future probability distribution of an initially known distribution. Trajectories of the released particles from the initial box are shown in green.

Figure 10. A solution for probability distribution of a source region. For proper forward-time integration, the starting time is shifted to $t_0 - T$. Virtual particles are released from *all* the boxes in the domain. Important particles are those who land in the target box which include the sampling location. Trajectories of particles which land in the target box are shown by green, other trajectories are shown by red. A solution for the probabilistic source region is conceptually the same as the solution of backward Kolmogorov equation where an initial probability distribution is the desired solution such that in a future time the system will have a specified probability distribution.
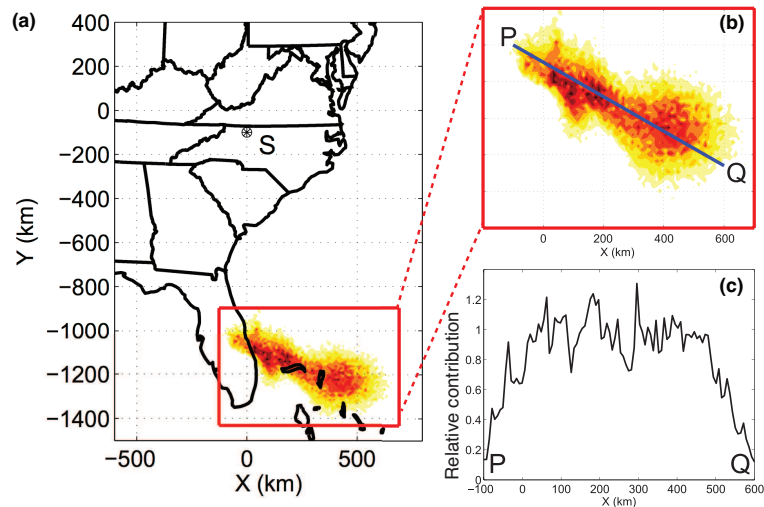
Figure 11. (a) The probabilistic equivalent of the source point of the green particle in Fig. 8. The sampling point S is located at (0, −100) km with respect to our reference point and sampling time is 14:10 UTC 29 September 2010, **(b)** details of the probabilistic source region which is composed of 5400 boxes, each 10 km × 10 km. Color intensity shows the relative contribution of each source box. **(c)** γ, relative contribution of source boxes along the specified line PQ.
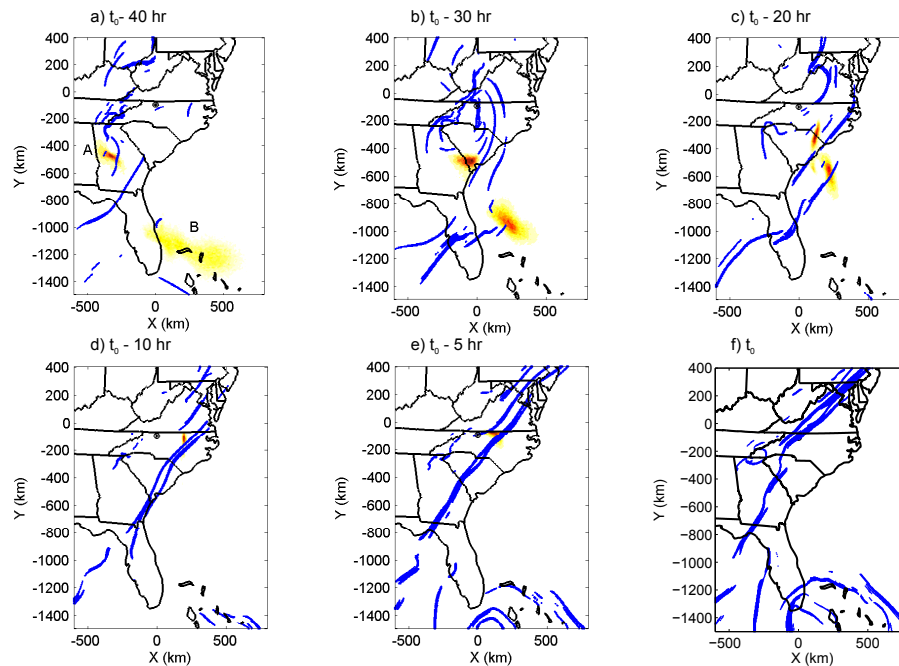
Figure 12. Sequence of hyperbolic LCSs (blue) and two probabilistic source regions corresponding to two successive samples. Probabilistic regions "A" and "B" **(a)** correspond to the virtually red and blue particles in Fig. 8. These six panels correspond to 40, 30, 20, 10, 5 and 0 h before collecting the corresponding samples at 13:40 and 14:00 UTC during the interrogation window.